



Impact of air-sea drag coefficient for latent heat flux on large scale climate in coupled and atmosphere stand-alone simulations

Olivier Torres¹ · Pascale Braconnot¹ · Olivier Marti¹ · Luc Gential^{1,2}

Received: 24 October 2017 / Accepted: 3 May 2018 / Published online: 11 May 2018
© Springer-Verlag GmbH Germany, part of Springer Nature 2018

Abstract

The turbulent fluxes across the ocean/atmosphere interface represent one of the principal driving forces of the global atmospheric and oceanic circulation. Despite decades of effort and improvements, representation of these fluxes still presents a challenge due to the small-scale acting turbulent processes compared to the resolved scales of the models. Beyond this subgrid parameterization issue, a comprehensive understanding of the impact of air-sea interactions on the climate system is still lacking. In this paper we investigate the large-scale impacts of the transfer coefficient used to compute turbulent heat fluxes with the IPSL-CM4 climate model in which the surface bulk formula is modified. Analyzing both atmosphere and coupled ocean–atmosphere general circulation model (AGCM, OAGCM) simulations allows us to study the direct effect and the mechanisms of adjustment to this modification. We focus on the representation of latent heat flux in the tropics. We show that the heat transfer coefficients are highly similar for a given parameterization between AGCM and OAGCM simulations. Although the same areas are impacted in both kind of simulations, the differences in surface heat fluxes are substantial. A regional modification of heat transfer coefficient has more impact than uniform modification in AGCM simulations while in OAGCM simulations, the opposite is observed. By studying the global energetics and the atmospheric circulation response to the modification, we highlight the role of the ocean in dampening a large part of the disturbance. Modification of the heat exchange coefficient modifies the way the coupled system works due to the link between atmospheric circulation and SST, and the different feedbacks between ocean and atmosphere. The adjustment that takes place implies a balance of net incoming solar radiation that is the same in all simulations. As there is no change in model physics other than drag coefficient, we obtain similar latent heat flux between coupled simulations with different atmospheric circulations. Finally, we analyze the impact of model tuning and show that it can offset part of the feedbacks.

Keywords Latent heat flux · Bulk parameterization · Sensitivity tests · Atmospheric heat transport · Ocean–atmosphere coupling · Climate simulations

1 Introduction

The ocean forms key component of the climate system. It has a major contribution in the equator-to-pole heat transport (Covey and Barron 1988) and in the feeding of the atmospheric water cycle (Chahine 1992). In the tropics the ocean and atmosphere are mainly coupled through two

large-scale atmospheric circulation systems: the Hadley and Walker circulations (Cao et al. 2015) which are driven by the heat and momentum exchanges at the air-sea interface and impact most of the globe (Trenberth 1995). These turbulent fluxes represent the main coupling between ocean and atmosphere and establish the link between ocean-surface temperature changes and atmospheric circulation variability (Kubota et al. 2002). They also provide the mechanism by which ocean variability is forced by the atmosphere. With the exception of surface roughness and albedo, sea surface temperature (SST) is the only oceanic variable that directly affects the atmosphere. SST is a key variables for the prediction of future climate variations (Seager et al. 1995) and is regulated by heat and momentum fluxes which contribute to the turbulent mixing within the ocean (Barnier 1998). The

✉ Olivier Torres
olivier.torres@lsce.ipsl.fr

¹ Laboratoire des Sciences du Climat et de l'Environnement, LSCE/IPSCL, CEA-CNRS-UVSQ, Université Paris-Saclay, 91191 Gif-sur-Yvette, France

² Present Address: Weathernews France SAS, 79 rue du Faubourg Poissonnière, 75009 Paris, France

turbulent momentum flux is the source of the wind-driven circulation of the upper ocean (Chen et al. 1994) and the transfer of heat across the air-sea interface determines the distribution of temperature and salinity in the ocean (Swenson and Hansen 1999). Globally averaged, the turbulent latent heat flux represents one of the largest contributions to the heat loss of the ocean. This flux is highest in the tropics where warm conditions prevail and regulates the adjustment between ocean and atmosphere by controlling the energetic balance and the amount of water available in the atmosphere. Improved understanding of the air-sea turbulent fluxes and their representation in climate models is therefore essential. This requires not only the representation of the fluxes themselves but also the mechanisms underlying energy and water adjustments between the ocean and atmosphere.

Compared to the resolved scales of the models, turbulent fluxes are subgrid scale phenomena and need to be parameterized. The understanding of air-sea fluxes is based on Monin–Obukhov similarity theory (Monin and Obukhov 1954) for surface boundary layers. In large-scale global numerical models, these fluxes are calculated using bulk formulae (Zeng et al. 1998). These are empirical equations that seek to represent, using large-scale variables, the air-sea fluxes generated by complex turbulent processes in the boundary layer (Large and Pond 1981; DeCosmo et al. 1996). The most common parameterization is to determine transfer coefficients as a function of wind speed and surface air stability (Blanc 1985; Smith 1988). One of the principal difficulties is the choice, or computation, of the exchange (drag) coefficients that appear in bulk formulae. Bulk formulae have difficulties in representing air-sea fluxes across all wind ranges (mainly low and high wind speed regimes) due to buoyancy effects on turbulent transport (Birol Kara et al. 2000) and therefore a large number of schemes are currently in use (Large and Yeager 2004; Fairall et al. 2003; Birol Kara et al. 2000). Such parameterizations represent a source of considerable uncertainty regarding the reliability of model simulations and forecasts (Seager et al. 1995). In atmospheric general circulation models (AGCM), the SST is required in the prognostic equation for surface air temperature. This is in turn necessary to calculate vertical fluxes through the planetary boundary layer of the atmosphere (Stull 1988). Climate simulations have been shown to be sensitive to the exchange coefficient. Depending on the parameterization, transition to free convective regimes (Miller et al. 1992) and various high frequency processes such as wind gustiness (Redelsperger et al. 2000) or wind waves (Fairall et al. 2003) are considered. In a coupled ocean–atmosphere model, turbulent fluxes are determined internally and are fully interactive with the simulated SST and near-surface atmospheric field. Because of this, it is difficult to disentangle the exact role of the fluxes on climate due to the feedbacks between ocean and atmosphere

or between the fluxes and the other atmosphere or oceanic parameterizations in climate models.

Hourdin et al. (2015) show that the biases in surface evaporation, specifically the biases in latent heat flux play as strong a role as cloud radiative effects in controlling the intensity of the eastern Pacific and Atlantic tropical ocean SST warm biases in CMIP5 simulations. Găinușă-Bogdan et al. (2018) highlight this relationship between the pattern of latent heat flux biases developed in forced atmospheric simulations and the SST biases present in coupled modes. This key relationship was not found previously because the ocean–atmosphere adjustment in coupled models suggested a different relationship between SST and latent heat fluxes, which corresponds in most regions to a response of the latent heat to SST and not the response of SST to the latent heat flux. These studies show that there is still a lack of understanding of the role played by turbulent fluxes in the adjustment between ocean and atmosphere and that there is a need to further investigate how the representation of these fluxes affects the results of climate change simulations.

This study aims to better understand the large-scale impacts of the turbulent fluxes and of their parameterization in global climate models by considering coupled and uncoupled simulations with a low atmospheric resolution version of the IPSL climate model (Marti et al. 2010). Sensitivity experiments to changes in the computation of the heat drag coefficient allow us to explore how changes in the latent heat flux parameterization affect the patterns and magnitudes of the simulated heat fluxes and of the variables used to compute them. Focusing on the atmospheric moist static energy balance, we relate surface changes to the redistribution of heat from source to sink regions and to analyze the coupled ocean atmosphere adjustment. Section 2 presents the model used for this study, the theoretical framework and the modifications introduced in the bulk formulations to performed sensitivity experiments. Section 3 present the results of the simulations obtained with an atmospheric stand-alone model (AGCM) while Sect. 4 present the results of the simulations obtained with an ocean–atmosphere coupled system (OAGCM) and a focus on the effect of model tuning. The main conclusions are given in Sect. 5.

2 Model and experiments

2.1 The IPSL-CM4 “Modèle Grande Vitesse” (MGV)

The model used in this study is the MGV version of the IPSL-CM4 coupled ocean–atmosphere model (Marti et al. 2010). It couples LMDZ-4 (Hourdin et al. 2006) for atmospheric dynamics and physics, NEMO-OPA (ORCA2.0 grid) for ocean dynamics (Madec et al. 1998), ORCHIDEE for terrestrial vegetation (Krinner 2005), and LIM (Fichefet and

Morales Maqueda 1999) for sea ice. In this configuration the atmosphere-land resolution is degraded to 44×44 grid points on the horizontal plane and 19 vertical levels. The ocean resolution (2°) is the same as in the standard IPSL-CM4 model. The AGCM reference (ASTD, Table 2) is a 11 year simulation performed using climatological SST's i.e. without interannual variations as described in Hourdin et al. (2006). For aerosols, greenhouse gases and continental surfaces a repeated 1980 climate is used. The OAGCM reference (CSTD, Table 2) is a 100 year simulation. The ocean initial state comes from the end of a 500 year reference simulation described in Marti et al. (2010) where the ocean is at equilibrium with the forcing conditions. The atmospheric initial state come from the last year of the AGCM (ASTD) simulation. The climatologies are computed from the last 10 years of simulation for the AGCM and from the last 40 years of the OAGCM simulation.

Figure 1 presents the climatological annual mean for precipitation, wind speed at 10 m and sea surface temperature for the reference simulation with the standard IPSL-CM4 (2L24, Marti et al. 2010), the reference simulation for the MGV (CSTD) and the observations. The observations comes from GPCP for precipitation (Adler et al. 2003), ERA-40 reanalysis for wind speed (Uppala et al. 2005) and HadISST1 for SST (Rayner 2003). Despite its low atmospheric

resolution, the MGV simulation is similar to the IPSL-CM4 reference. It represents the large-scale patterns of sea surface temperature and precipitation (Fig. 1). Compared to the observations, the warm pool is too wide in latitude and the well-known east coast warm bias is present both in CSTD and 2L24 simulations. Compared to the 2L24 simulation, the warm pool is less eroded in CSTD however the Atlantic Ocean is too warm. A less pronounced double ITCZ (Inter-Tropical Convergence Zone) and more intense precipitation around the maritime continent is also observed for CSTD compared to 2L24. This is due to the smoothing of the SST pattern on the atmospheric grid, which dampens local feedbacks between SST, wind convergence, precipitation and radiation that contribute to the development of the double ITCZ in the IPSL model (Bellucci et al. 2010). For wind speed, the large-scale structures are represented but in middle and high latitudes winds are not strong enough in storm track regions in the CSTD simulation compared to both 2L24 and observations. The MGV underestimates ocean heat transport in the northern hemisphere (Fig. 2). This is due to the slowdown of the thermohaline circulation caused by low wind speeds and associated reduced gyre circulation that brings less warm and high salinity water from the tropics to the North Atlantic Ocean convection sites. With the exception of this bias, ocean atmosphere heat transport

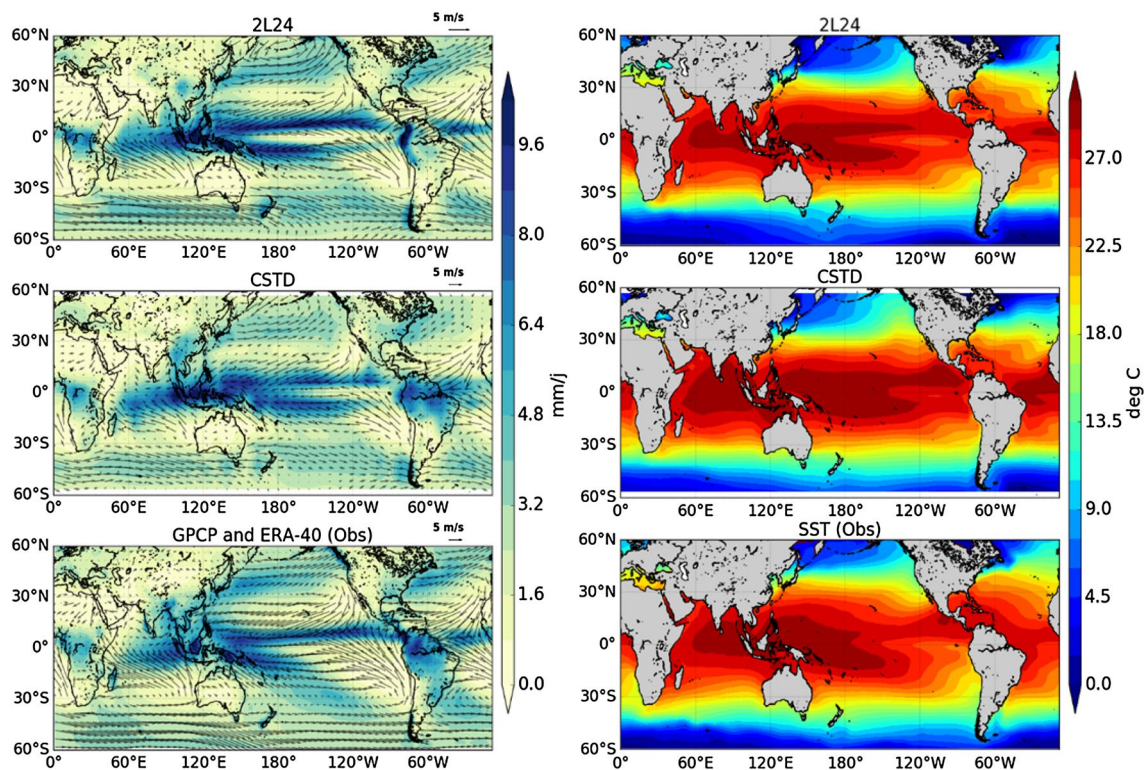


Fig. 1 Annual mean precipitation (mm/day) and surface wind (m/s) (left) and SST (right) for the MGV reference CSTD (up), the IPSL-CM4 reference 2L24 (middle) and observations (bottom)

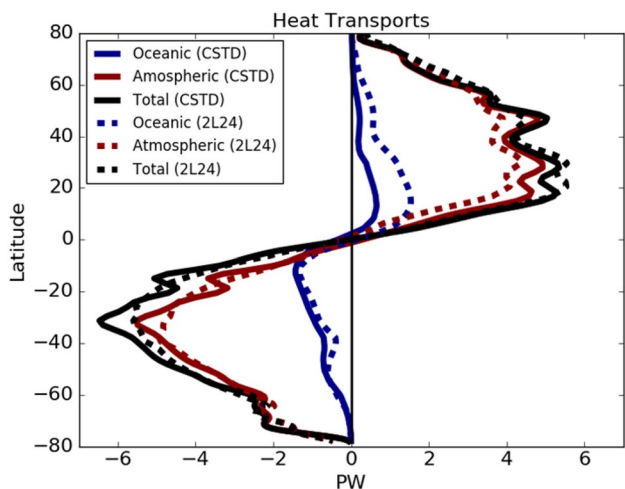


Fig. 2 Meridional heat transport (PW) considering the total heat transport (black) and the atmosphere (red) and ocean (blue) contribution. The solids line stand for the MGV CREF simulation and the dotted lines for the IPSL-CM4 2L24 reference

is well represented with the correct order of magnitude respected.

This short comparison highlights that the MGV model represents the large-scale phenomena although with deficiencies related to its resolution and to IPSL-CM4 physics. The MGV and the computational advantages it represents is thus an efficient compromise for this study where we consider first order large scale adjustments between ocean and atmosphere. We are confident that the results will remain valid at higher resolutions.

2.2 Theoretical framework

At the scale of a GCM (general circulation model) mesh, turbulence is not explicitly resolved and needs to be parameterized. For this purpose an analogy with the diffusion equations at the molecular scale is made. The turbulent diffusion is estimated from resolved large-scale variables (Corrsin 1975), according to Monin–Obukhov’s theory of similarity (Monin and Obukhov 1954). In the IPSL-CM4 model (Marti et al. 2010) the latent heat flux is calculated as follows:

$$L_{ve} = -\rho_a L_v C_Q (U_1 - U_s)(q_1 - q_s) \tag{1}$$

where L_v is the latent heat of vaporization (J/kg), ρ_a is the air density (kg/m³), U_1 and U_s represent respectively wind speeds at the first vertical model level and the surface (m/s), C_Q is the transfer coefficient and, q_s and q_1 represent specific humidity (kg/kg) at the surface and at the first vertical model level respectively.

For each flux there is theoretically a corresponding transfer coefficient, C_D for roughness, C_Q for latent heat and C_H for sensible heat (Louis 1979; Beljaars and Beljaars 1995).

Over the continents, surface roughness length is calculated as a function of surface land cover and is given by the land surface model according to vegetation type. In the following we only consider the oceanic part of the system in sensitivity experiments.

Over the ocean, the transfer coefficient for momentum is expressed as follows:

$$C_D = C_{DN} * f(R_i) = \frac{\kappa^2}{\log\left(1 + \frac{z}{z_{0m}}\right)^2} * f(R_i) \tag{2}$$

with:

$$z_{0m} = \frac{0.11 * v}{u_*} + \frac{0.018 * u_*^2}{g} \tag{3}$$

$$R_i = \frac{f \Delta z \Delta \theta_v}{\theta_v |\Delta u|^2} \tag{4}$$

where C_{DN} is the neutral coefficient, v is the kinematic viscosity, u_* is the friction velocity, $f(R_i)$ is a stability function derived from the stability of the atmosphere determined by the Richardson number (4), κ is the von Kármán constant (=0.4), z is the height of the first layer of the model and z_0 is the roughness length (3) based on (Smith 1988) through the Charnock formula (Charnock 1955) which takes into account the aerodynamic roughness height of the surface $\left(\frac{0.018 * u_*^2}{g}\right)$ and the roughness length for a smooth surface $\left(\frac{0.11 * v}{u_*}\right)$.

In the model, the stability function $f(R_i)$ is different in stable and unstable cases. Over the ocean a low wind speed parameterization is used for the heat transfer coefficient. It mimics the transition to free convection regimes over low wind speed unstable regimes (Miller et al. 1992). For sensible and latent heat, the drag coefficient over the ocean is:

Stable case : $C_D = C_{DN} * f(R_i)$ and $C_H = C_Q = 0.8 * C_D$ (5)

Unstable case : $C_D = C_{DN} * f(R_i)$ and $C_H = C_Q = 0.8 * C_D * (1 + C_R^\gamma)^{\frac{1}{\gamma}}$ (6)

With $C_R = \frac{0.0016}{C_{QN} |U_1|} (\theta_{vs} - \theta_{vl})^{\frac{1}{\gamma}}$ and $\gamma = 1.25$ (Miller et al. 1992).

Note that in the parameterization used in this study the bulk transfer coefficients for sensible heat (C_H) and for water vapor (C_Q) are equal as shown in Eqs. 5 and 6. In the following, C_H refers to both of these transfer coefficients. In addition, it is important to note that the 0.8 coefficient used

in Eqs. 5 and 6 has been introduced to take into account the differences between the momentum transfer coefficient and the transfer coefficients for water vapor and sensible heat in a version of the model in which it was not possible to implement a full parameterization of sensible heat and water vapor transfer coefficients (Marti et al. 2010).

2.3 Sensitivity experiment to bulk parameterization

In order to test the impact of the heat transfer coefficients and thus of the bulk parameterizations, several idealized sensitivity tests were carried out on the various characteristics of the C_H parameterization in forced mode (AGCM) with prescribed SST as well as in coupled mode (OAGCM). Starting from the reference simulations ASTD and CSTD the different simulations have slight modifications of the exchange coefficient parameterization (Table 1). Each simulation realized in this study has a specific objective. The first simulation focuses on the impact of the separating factor used to differentiate C_D and C_H (AREF, CREF). The second explores the impact of a change in the neutral coefficient (ACTN, CCTN). The third addresses the impact of wind dependency on the heat exchange coefficient (ACTU, CCTU). Finally, the fourth simulation focuses on the importance of the low wind speed parameterization as in Miller et al. (1992) (ANLW, CNLW). It should be noted that the

perturbations initiated for the various sensitivity tests only impact the transfer coefficients for heat (C_H). The calculation of the momentum transfer coefficient (C_D) remains identical in all simulations. AGCM sensitivity experiments have the same climate forcing as ASTD and a duration of 10 years. For the OAGCM sensitivity simulations, the atmospheric initial state is the last year of the corresponding AGCM simulation, whereas the oceanic initial state is the same as for CSTD. The OAGCM simulations have a duration of 100 years. The objective is not to run the model to equilibrium but to understand the different model adjustments.

Figure 3 presents the transfer coefficients for heat (C_H) as a function of wind speed for the different simulations. The effects of the modification of the parameterization are the same between the simulations carried out with the AGCM (Fig. 3a) and the fully coupled system (Fig. 3b). This confirms that similar wind regimes and physics are active in coupled and in the corresponding atmosphere stand-alone simulations. The reference simulations ASTD, CSTD have a transfer coefficient about 17% lower than the simulations AREF, CREF as expected from the removal of the separating factor (0.8) in the parameterization. The differences between AREF, CREF and ACTN, CCTN come from the introduction of a fixed neutral coefficient that increases C_H by about 25% (Table 2). Removing the low wind speed parameterization (ANLW, CNLW) leads to a strong decrease of about 19% in the transfer coefficient.

Table 1 Set up of each different bulk parameterization

Mode	Name	Low wind speed function	Neutral coefficient over ocean for C_Q and C_H	Heat transfer coefficients over ocean (C_Q, C_H)
Forced	ASTD	On	$\frac{\kappa^2}{\log\left(1 + \frac{z}{z_{0m}}\right)^2}$	Stable: $0.8 * C_D^*$ stability Unstable: $0.8 * C_D * (1 + C_R^y)^{\frac{1}{7}}$ stability
	AREF	On	$\frac{\kappa^2}{\log\left(1 + \frac{z}{z_{0m}}\right)^2}$	Stable: C_D^* stability Unstable: $C_D * (1 + C_R^y)^{\frac{1}{7}}$ stability
	ACTN	On	0.0011	Stable: C_D^* stability Unstable: $C_D * (1 + C_R^y)^{\frac{1}{7}}$ stability
	ACTU	Off	$\frac{\kappa^2}{\log\left(1 + \frac{z}{z_{0m}}\right)^2}$	Stable: C_D^* stability Unstable: 0.0011
	ANLW	Off	$\frac{\kappa^2}{\log\left(1 + \frac{z}{z_{0m}}\right)^2}$	Stable: C_D^* stability Unstable: C_D^* stability
Coupled	CSTD	On	$\frac{\kappa^2}{\log\left(1 + \frac{z}{z_{0m}}\right)^2}$	Stable: $0.8 * C_D^*$ stability Unstable: $0.8 * C_D * (1 + C_R^y)^{\frac{1}{7}}$ stability
	CREF	On	$\frac{\kappa^2}{\log\left(1 + \frac{z}{z_{0m}}\right)^2}$	Stable: C_D^* stability Unstable: $C_D * (1 + C_R^y)^{\frac{1}{7}}$ stability
	CCTN	On	0.0011	Stable: C_D^* stability Unstable: $C_D * (1 + C_R^y)^{\frac{1}{7}}$ stability
	CCTU	On	$\frac{\kappa^2}{\log\left(1 + \frac{z}{z_{0m}}\right)^2}$	Stable: C_D^* stability Unstable: 0.0011
	CNLW	Off	$\frac{\kappa^2}{\log\left(1 + \frac{z}{z_{0m}}\right)^2}$	Stable: C_D^* stability Unstable: C_D^* stability

Fig. 3 Transfer coefficient for heat over ocean ($C_H, *10^{-3}$) as a function of the wind speed for **a** AGCM's and **b** OAGCM's simulations

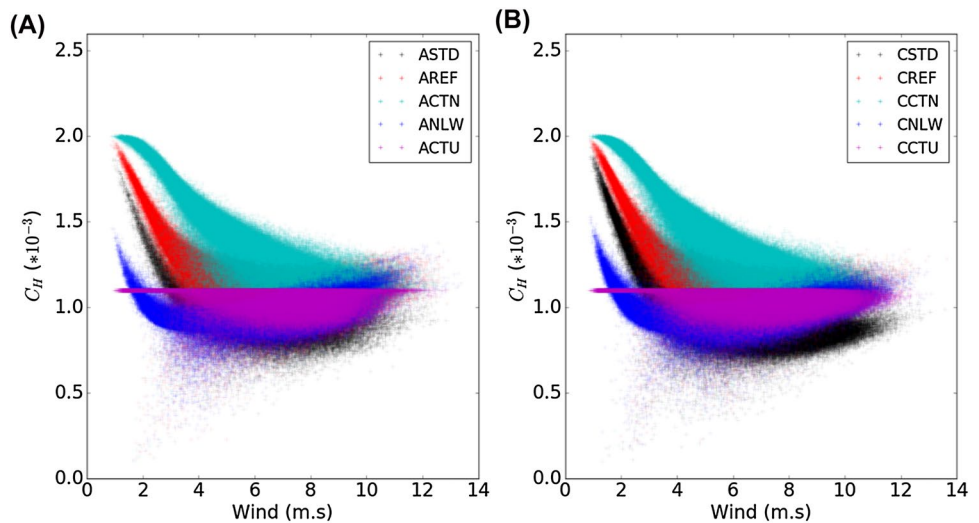


Table 2 Spatio-temporal averages between 20°N and 20°S of heat exchange coefficient $C_H (*10^{-3})$, latent heat flux (W/m^2) and precipitation (mm/day), together with the % change compared to the reference. The last column is the global average of net radiative flux at

top of atmosphere (TOA) that provide a measure of the global climate equilibrium of the model. Note that the error bar (\pm) is compute from the last 40 years for the coupled simulations and from the 10 years of simulation for AGCM's simulations

Mode	Name	$C_H (*10^{-3}) \pm 0.01$	%	Latent heat flux (W/m^2) ± 3.3	%	Precipitations (mm/day) ± 0.31	%	Net TOA (W/m^2) ± 0.6
AGCM	AREF	1.18	0.00	136.20	0.00	3.69	0.00	-2.47
	ASTD	0.97	-17.72	128.30	-5.80	3.43	-7.23	-0.51
	ACTN	1.48	25.38	145.30	6.68	4.09	10.78	-4.49
	ACTU	1.10	-6.62	130.10	-4.48	3.62	-1.95	-0.46
	ANLW	0.96	-18.75	124.10	-8.88	3.34	-9.64	0.84
Mode	Name	$C_H (*10^{-3}) \pm 0.01$	%	Latent heat flux (W/m^2) ± 1.9	%	Precipitations (mm/day) ± 0.16	%	Net TOA (W/m^2) ± 0.28
OAGCM	CREF	1.22	0.00	132.50	0.00	3.78	0.00	-0.43
	CSTD	1.01	-16.78	134.00	1.13	3.85	1.93	0.59
	CCTN	1.51	23.93	129.30	-2.42	3.58	-5.26	-1.43
	CCTU	1.10	-9.54	133.50	0.75	3.83	1.35	-0.12
	CNLW	0.98	-19.76	134.50	1.51	3.90	3.12	0.22

When this is active, it reinforces C_H for low wind speed values as expected but it should be noted that this function also affect C_H for wind speeds greater than 5 m/s (Fig. 3). Finally, for the simulations ACTU, CCTU the transfer coefficient decreases by about 8% compared to AREF, CREF. These simulations have the lowest transfer coefficient for very low wind speeds (<2 m s), in the unstable cases the C_H is fixed at 0.0011 and in the stable cases, the values of C_H approximates the values of ANLW, CNLW.

The model version equivalent to the IPSL-CM4 (2L24 simulation) is used for ASTD and CSTD (for AGCM and OAGCM). However in this study, to overcome the effect of the coefficient (0.8) used to separate the transfer coefficients that is only present in ASTD and CSTD, we consider AREF

and CREF as reference simulation for atmosphere alone and coupled ocean-atmosphere simulations respectively.

3 Impact of bulk formulae on AGCM simulations

3.1 Annual mean changes

Figure 4 shows the long-term mean changes in latent heat flux (LH, W/m^2), rainfall (Pr, mm/day), specific humidity at the first atmospheric level (H, g kg) and the transfer coefficient (C_H) compared to the reference (AREF). The tropics, where evaporation is the strongest, are the most affected by

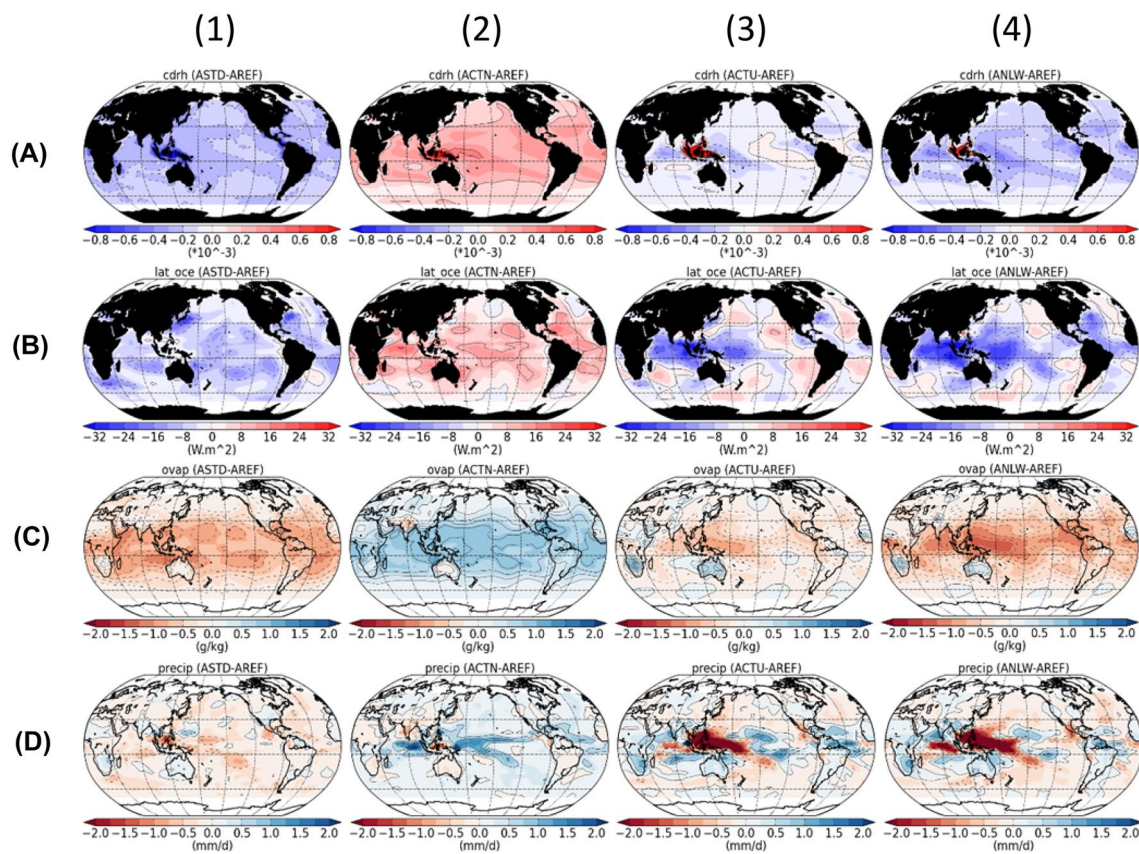


Fig. 4 Annual mean differences between (1) ASTD and AREF, (2) ACTN and AREF, (3) ACTU and AREF and (4) ANLW and AREF for **a** C_H , **b** latent heat fluxes (W/m^2), **c** humidity at 1st level (g/kg) and **d** precipitation (mm/day)

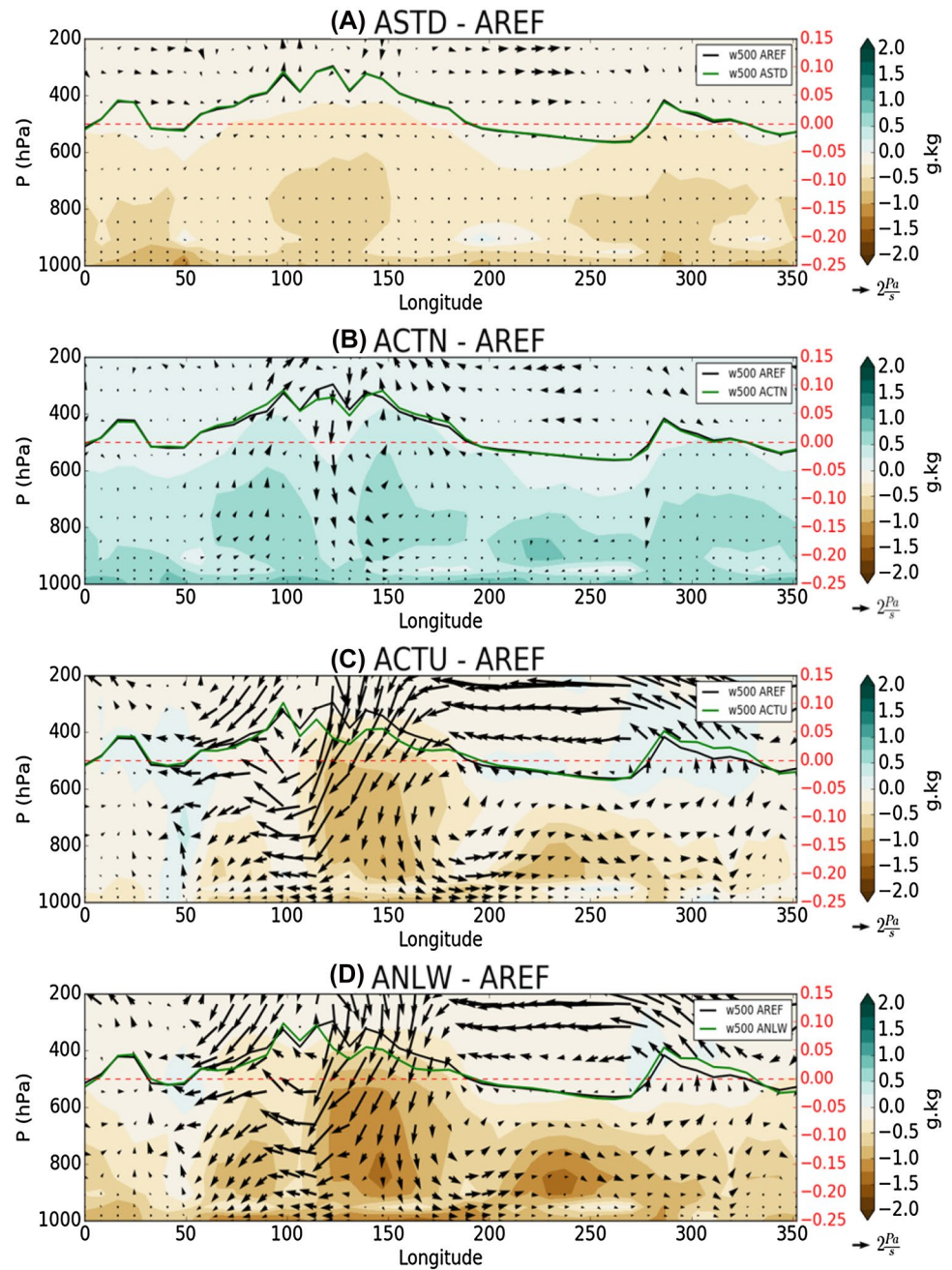
the modification in the bulk formulae (Fig. 4). With imposed SST and humidity at the ocean surface, the model reacts as expected. An increase (decrease) in the transfer coefficient leads to an increase (decrease) of the latent heat flux and thereby of precipitation and specific humidity at the first model level (Fig. 4).

Table 2 summarizes the spatio-temporal averages over the tropics (10 year averages between $20^{\circ}S$ and $20^{\circ}N$) of C_H , LH, Pr, net radiative balance at the top of atmosphere (TOA) and the relative increases/decreases (in %) with respect to the reference simulation. All simulations, except ACTN, reduced C_H with the largest reduction obtained for ANLW with a decrease of 18.8% in the heat transfer coefficient (ANLW, Table 2). This reduction leads to a decrease of 8.9% in the latent heat flux and a decrease of 9.6% in precipitation, impacting the global radiative balance at the top of atmosphere (Table 2). Compared to the reference, the tropics are colder and drier for ANLW ($-0.7^{\circ}C$ and -0.35 mm/day). With the exception of ACTN [where the tropics are warmer and wetter ($+0.5^{\circ}C$ and $+0.4$ mm/day)], the other simulations exhibit similar behaviors (Table 2). The imposed changes in the drag coefficient impose a change that has almost no impact on the pattern of the simulated

latent heat flux or a change that causes regional difference compared to the reference simulation (Fig. 4). This explains why changes between the different variables at the scale of the tropics are not proportional from one simulation to the other. In particular, ASTD and ANLW have close values for the change in latent heat drag coefficient but ASTD simulates 7.23% and ANLW 9.64% (Table 2) less precipitation compared to the reference (AREF).

For ASTD and ACTN, the change in the transfer coefficient is spatially homogeneous and leads to an increase (decrease) of the latent heat flux almost everywhere (Fig. 4 1b, 2b). This implies an enhancement (reduction) of the humidity over the entire tropics (Fig. 4 1c, 2c). When SST is imposed, such changes do not alter large-scale humidity or temperature gradients and do not cross thresholds that would modify the atmospheric circulation or stability and thereby atmospheric convection. Consequently, the variation of the transfer coefficient has no impact on vertical velocity or the large-scale Walker circulation (Fig. 5a, b). We only notice an increase (decrease) in precipitation in the tropical band where the ITCZ is located due to the modification of humidity (Fig. 4 1d, 2d).

Fig. 5 Annual mean differences between **a** ASTD and AREF, **b** ACTN and AREF, **c** ACTU and AREF and **d** ANLW and AREF averaged between 5°N and 5°S for humidity (colors, g/kg), wind (arrows, Pa/m s) and vertical velocity at 500 hPa where the black lines stands for the reference simulation (AREF) and the green line for the sensitivity experiment (Pa/s). Note that on these figures the vertical velocity has been magnified by a factor 100 and the sign has been reversed so that descending (ascending) arrows indicate subsidence (ascent)



Conversely, for ANLW and ACTU the change is more regional. Suppressing the low wind speed parameterization induces large-scale pattern changes in the heat transfer coefficient over the warm pool and Indo-Pacific sectors where low winds are found (Fig. 4 3a, 4a). This implies a decrease in the latent heat flux and therefore a reduction in humidity in the first atmospheric layers. Global precipitation decreases. Over the Indian Ocean and west Pacific precipitation declines by more than 2 mm/day while it increases over the western parts of the Pacific and Atlantic oceans (Fig. 4 3c 3d). Figure 5c, d shows that it affects the whole atmospheric column and is associated with a decrease in the

upward branch of the Walker cell in the warm pool region and with reduced atmospheric convection as can be deduced from the reduced upward vertical velocity at 500 hPa. The large-scale linkages between convection and winds in the tropics is such that the surface wind is also reduced. This comparison shows that depending on the pattern of C_H changes and the linkages with change in humidity and atmospheric convection, different zonal wind speeds correspond to the same imposed SST gradients at the surface.

These differences in latent heat between the east and west of the Pacific basin which depend on the change in CH are also found in the net surface fluxes calculated as

the sum of the latent, sensible and radiative fluxes. We define two boxes between 30°N and 30°S, one in the in the west Pacific (60°–180°E) and one in the east Pacific (180°–80°W). Figure 6 presents the spatio-temporal average differences for ASTD and ANLW compared to the reference (AREF) in these two boxes for the net surface flux and its different components. In this figure, although included in the calculation of the net surface flux, the sensible heat flux is not shown because in tropical regions it is an order of magnitude lower than the other components.

In the west Pacific box the mean anomaly value of the net surface flux is -1.99 and -19.1 W m^2 while in the east box is -3.28 and -1.89 W m^2 respectively for ASTD and ANLW compared to the reference. In both boxes, the latent heat flux dominates the net radiative flux (-6.87 and -16.19 W m^2 in the west and -7.95 and -7.5 W m^2 in the east respectively for ASTD and ANLW). The effect of latent heat flux is reinforced by the shortwave surface flux (-0.89 and -8.69 W m^2 in the west and -2.29 and -2.76 W m^2 in the east respectively for ASTD and ANLW) and counterbalanced by the long wave flux at surface (5.26 and 6.18 W m^2 in the west and 6.22 and 7.37 W m^2 in the east respectively for ASTD and ANLW). When we analyze the cloud radiative forcing (CRF) at the surface, we find that the change in solar radiation is due to reduced cloud cover. Indeed, the short-wave CRF accounts for most of the SW change (-0.11 and -8.03 W m^2 in the west box and -1.61 and -2.04 W m^2 in the east box). The long-wave CRF is almost negligible (Fig. 6), LW directly reflect the reduced humidity and associated reduced greenhouse effect. The changes observed in the AGCM simulations are mostly controlled by the modification of the latent flux. However, the west and east Pacific basins respond differently, a global change has stronger impacts in the east while the low wind parameterization (regional change) induces larger effects in the west (Fig. 6).

3.2 Equator-to-pole redistribution of energy

These changes in large-scale circulation and net radiative flux are related to large-scale differences in moist static energy (MSE) induced by surface latent heat changes. We consider the MSE, combining the dry static energy (heat plus potential energy) and the latent energy:

$$MSE = C_p T + gz + Lq \tag{7}$$

where C_p is the specific heat of air at constant pressure, T is the air temperature, g is the gravitational acceleration, z is the altitude, L is the latent heat of condensation and q is the specific humidity.

In an ocean atmosphere column at equilibrium, the annual mean net radiative flux RAD_{TOA} (positive downward) is balanced by the divergence of the MSE horizontal export out of the atmospheric column ($\vec{\nabla} \cdot \vec{F}_{MSE}$) and the divergence of the ocean heat horizontal export out of the oceanic column ($\vec{\nabla} \cdot \vec{F}_O$):

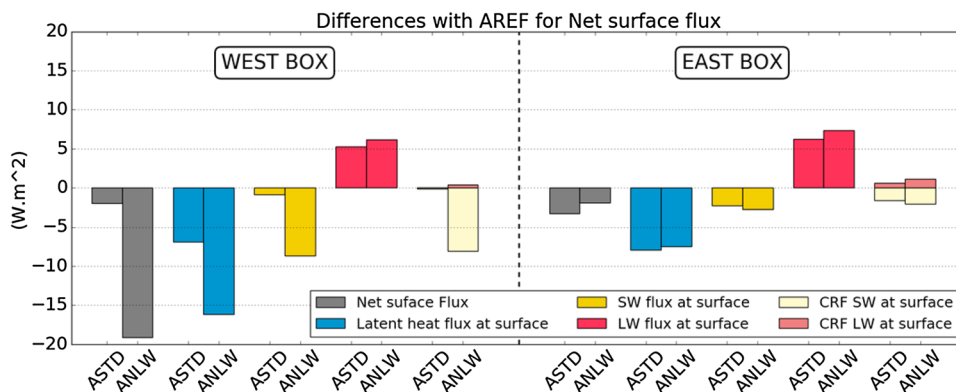
$$RAD_{TOA} = \vec{\nabla} \cdot \vec{F}_{MSE} + \vec{\nabla} \cdot \vec{F}_O \tag{8}$$

In this study, we only consider the horizontal export out of the atmospheric column ($\vec{\nabla} \cdot \vec{F}_{MSE}$).

The MSE horizontal transport (F_{MSE}) is computed as the divergent part of the MSE horizontal flux (Saint-Lu et al. 2016). The annual mean \vec{F}_{MSE} and its different components (dry static energy (DSE) and latent energy (Lq)) is shown in Fig. 7 for the reference AREF. Regions where the MSE potential is negative correspond to energy sources, whereas regions where it is positive correspond to energy sinks for the atmosphere. Figure 7a shows that atmospheric energy transports diverge from the tropics (the sources) and converge in high latitudes (the sinks). The warm pool, where the warmest water (SST) is found and where deep convection occurs, is the largest source of MSE. Energy is zonally transferred by the atmosphere from the warm pool to the other oceanic basins (Fig. 7).

As explained by Trenberth and Stepaniak (2004), the moisture in the atmosphere is transported (Lq export)

Fig. 6 Annual mean differences on net surface flux and its different components in two boxes for ASTD and ANLW compared to AREF. The west box correspond to a spatial average between 30°N, 30°S and 80°–180°E while the east box correspond to a spatial average between 30°N–30°S and 180°–80°W



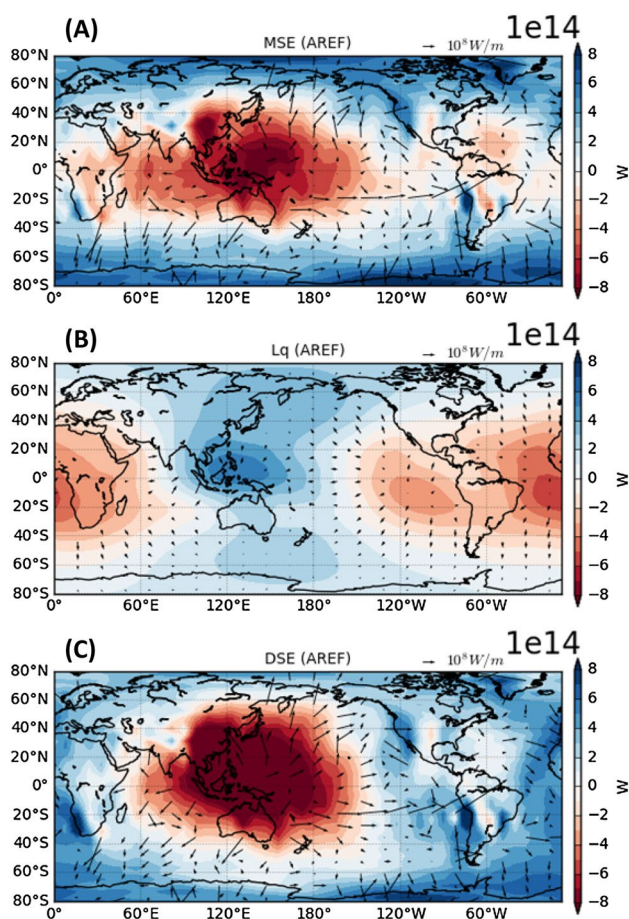


Fig. 7 Annual mean MSE transport by the atmosphere (arrows, W/m) and MSE potential (colors, W) (a), Lq transport by the atmosphere (arrows, W/m) and Lq potential (colors, W) (b) and DSE transport by the atmosphere (arrows, W/m) and DSE potential (colors, W) (c) for the reference simulation AREF. Arrows are drawn every 2 points on X and Y axis and continents are masked because of the too noisy continental signal due to low resolution

towards areas where the air is forced to raise (mostly around the warm pool) and hence cool. This explains the zonal export of energy from Atlantic and east Pacific basins to the warm pool regions by the latent energy (Lq, Fig. 7b). This phenomena results in a strong latent heating that drives the upward branch of the walker circulation located in this region. The DSE export is on the other hand linked with the upper atmospheric circulation. When the air rises, the moist energy is converted into sensible heat through the release of latent heat and is then exported poleward by the Hadley cells in the form of dry static energy (Fig. 7c). The warm pool thus is both a sink (Lq potential energy) and a source (DSE potential energy) of energy. The result is a net export of MSE to the poles and from the warm pool to the other basins (Fig. 7a–c).

Figure 8 depicts the long-term mean changes in MSE and Lq potential for ASTD and ANLW compared to the

reference (AREF). For ASTD the decrease in transfer coefficient does not change the atmospheric circulation (Fig. 5a). It only affects the atmospheric humidity, which decreases, but doesn't induce changes in Lq export (Fig. 8b). Consequently the differences in MSE export are very small (Fig. 8a) with only slight differences between the east and west of the Pacific basin. For ACTN (map not shown) the same behavior is observed but with opposite sign and slightly larger amplitude.

For ANLW the mean MSE export out of the warm pool region is reduced (Fig. 8c). This is consistent with the latent heat flux reduction over this region due to the suppression of the low wind speed parameterization that reduces heat and moisture availability for the atmosphere and leads to a decrease in the export of Lq from the other basins to the warm pool (Fig. 8d). This reduction in Lq potential is associated with an increase of MSE potential over the eastern part of the Pacific (negative value) and a decrease (positive value) over the western part (Fig. 8c). The eastern and western parts of the Pacific respond differently. This reflects the E/W gradient in latent heat flux (Fig. 4b) and the differences in net heat fluxes (Fig. 6). It also confirms that the change in Walker circulation balances the Lq and therefore the MSE exchange coming from the E/W gradient induced by latent heat changes at the surface. Latent heat flux control is therefore an important part of the exchange of energy between basins. For ACTU the same phenomenon is observed with a slightly lower amplitude.

The zonal integral of the heat transport (Fig. 9) confirms that the largest reduction of the equator-to-pole heat transport is obtained for ANLW and ACTU. For these two simulations, the largest differences are found between 20°S and 20°N and is associated with changes in the Hadley circulation. The change in atmospheric moisture increases the MSE transport in the south and decreases it in the north. It also shows that the latitude of maximum difference in latent heat transport strongly depends on whether the changes in latent heat induced by different drag coefficient parameterizations is homogeneous or has an E/W asymmetry in the Pacific ocean (Fig. 9).

The comparison of these simulations indicates that latent heat flux plays a key role on the atmospheric circulation and the exchange of energy between basins due to its impact on lower atmospheric layers. In an AGCM, the changes in latent heat directly reflect the way the heat exchange coefficients are represented. It is enhanced by radiative feedbacks due to the imposed SST and incoming solar radiation. Increasing (decreasing) the turbulent heat flux at the surface leads to an increase (decrease) of the radiative imbalance at the TOA (Table 2) of up to -4.49 W/m^2 for ACTN. This imbalance would lead to long-term adjustment when the atmosphere is coupled to the ocean as discussed below from the analysis of the same sensitivity test with the MGV

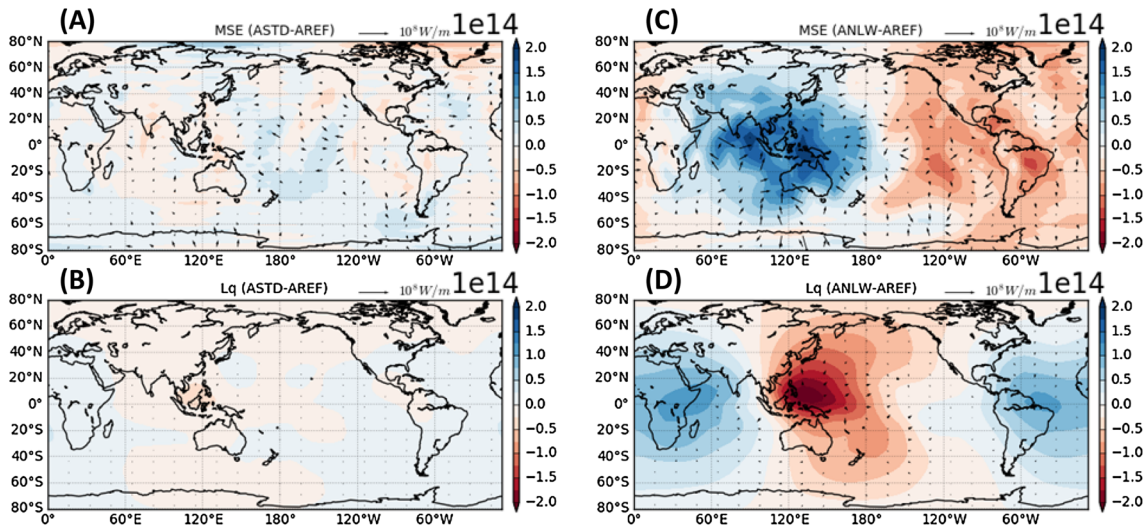


Fig. 8 Differences on the annual mean MSE and Lq transport by the atmosphere (arrows, W/m) and MSE and Lq potential (colors, W) between (a, b) ASTD and AREF and (c, d) ANLW and AREF.

Arrows are draw every 2 points on X and Y axis and continents are masked because of the too noisy continental signal due to low resolution

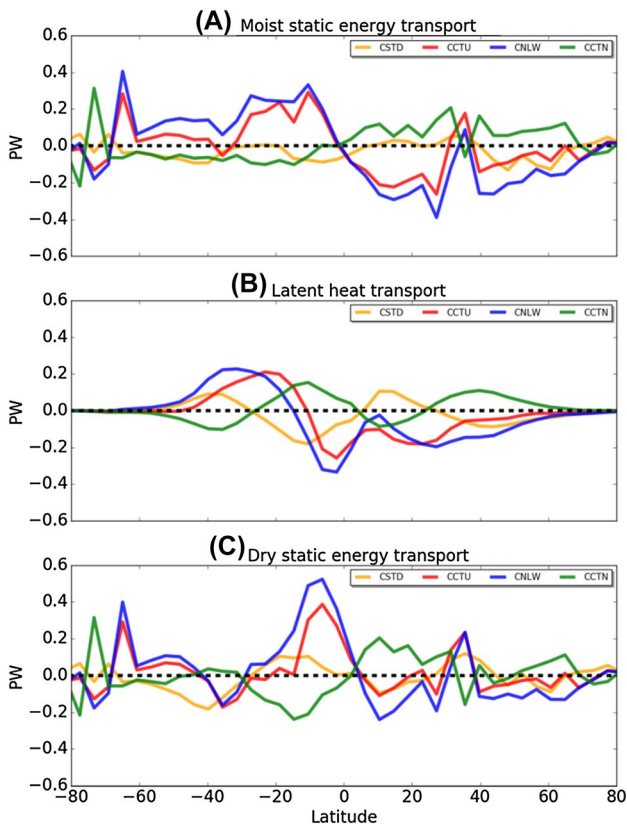


Fig. 9 Differences of a the annual mean MSE transport by the atmosphere (PW), b annual mean atmospheric latent heat transport (PW) and c annual mean dry static energy transport between ASTD, ACTN, ACTU, ANLW and AREF

OAGCM. Note that the simulation ASTD is almost equilibrated (-0.51 W/m^2) because it corresponds to the reference climate version (2L24). Our reference here is AREF with -2.47 W/m^2 resulting from the removal of the separating factor (0.8) and an increase in heat exchange coefficient (C_H). This need to be accounted for when discussing the OAGCM simulations below.

4 Impact of bulk formula on OAGCM simulations

4.1 Adjustment of the ocean atmosphere system

Figure 3b shows that the effect of the perturbations on the heat drag coefficient (C_H) is similar between the simulations carried out with the fully coupled system and the AGCM. The same physical processes are acting in the AGCM and OAGCM simulations. This is consistent with what is expected from the change in parameterizations. However, the effects observed on latent heat flux are opposite (Table 2; Figs. 4, 10). An increase in the transfer coefficient leads to a decrease in the latent heat flux and precipitation. Conversely, decreased C_H leads to an increase in latent heat flux and precipitation. As for the simulation carried out with the atmospheric stand-alone model, the tropical band is the most impacted by the perturbation (Fig. 10). For CCTN, precipitation decreases between 10°N and 10°S and increases between 40°N and 10°N and 40°S and 10°S while moisture decreases everywhere compared to the reference CREF. For CSTD, CNLW and CCTU the opposite is observed with a

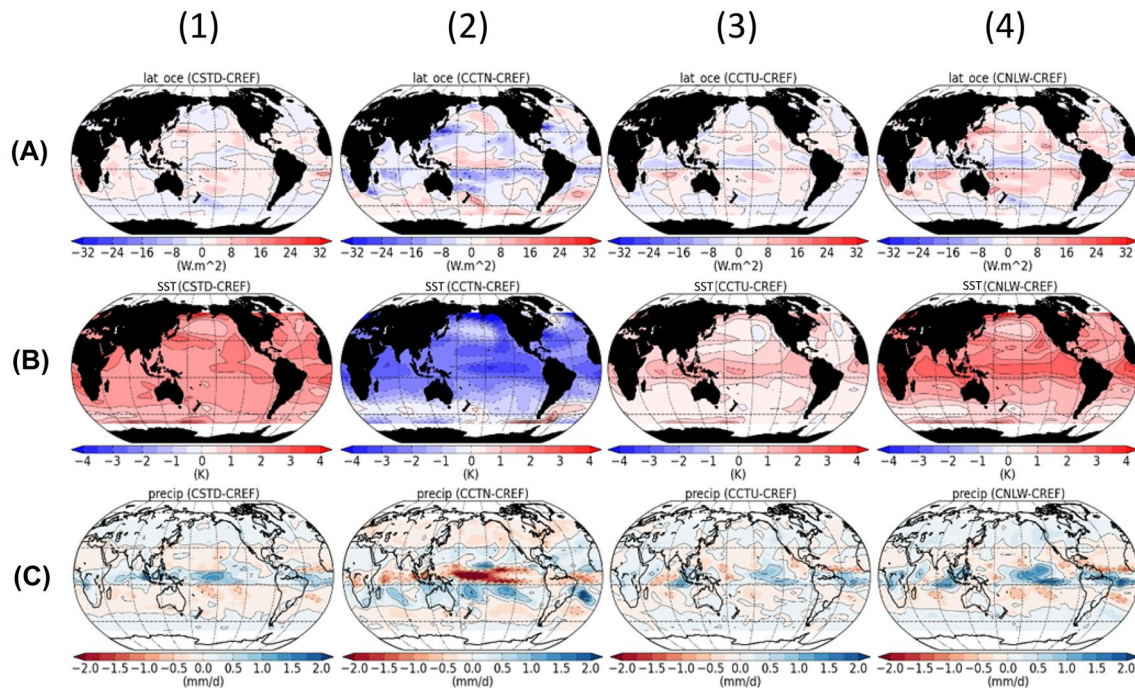


Fig. 10 Annual mean differences between (1) CSTD and CREF, (2) CCTN and CREF, (3) CCTU and CREF and (4) CNLW and CREF for **a** Latent heat fluxes (W/m^2), **b** SST ($^{\circ}\text{C}$) and **c** precipitation (mm/day)

lower intensity (Fig. 10). When we coupled the ocean and the atmosphere the perturbation induced by the modification of the heat drag coefficient had a direct impacts on SST. The ocean dampens the direct effect by absorbing or releasing energy and counteracting the initial perturbation. Modification of the SST leads to a destabilization of the humidity gradient that modifies the atmospheric circulation involving the link between SST and circulation highlighted in other studies (McGregor et al. 2014; Minobe et al. 2008). Subsequently, atmospheric and oceanic feedbacks modify the atmosphere ocean radiative equilibrium.

Figure 11 illustrates the ocean atmosphere adjustment. All sensitivity experiments start from the final year of the corresponding AGCM simulation and with the same initial ocean state. The radiative imbalance induced by the sensitivity test to C_H leads to rapid model drift. A negative (positive) heat budget at TOA corresponds to a cooling (warming). As an example, the $-2.47 \text{ W}/\text{m}^2$ radiative imbalance at TOA for AREF (Table 2) is seen at the beginning of the CREF simulation (Fig. 11a). After 40 years the imbalance at TOA declines as the ocean cools (Fig. 11a, c). The reduced SST is also associated with reduced air temperature and humidity following the Clausius–Clapeyron relationship (Fig. 11d). This corresponds to a reduction of 7.82% of humidity per degree for the CREF simulation. This value is similar to the ones obtains for global warming experiments ($7.5\%/K \pm 2\%$) (Held and Soden 2006). At the same time the reduced SST dampens the surface latent heat flux (Fig. 10b), which

explains why despite a much higher drag coefficient the latent heat flux is almost the same as in the other simulations (Table 2). This adjustment process leads to nearly the same global latent heat flux in all simulations (Fig. 11b) with different SST and other climate variables. The latent heat flux has a key role in determining Earth’s radiative equilibrium. As all simulations respond to identical incoming solar radiation, the latent heat needs to be almost identical to achieve global radiative balance. The adjustment of the ocean creates a modification of the state variables like temperature and humidity used to compute the turbulent fluxes. When the adjustment is almost complete, compared to the reference (CREF, Table 2), the tropics (20°S – 20°N) are colder and dryer for CCTN by about -2.1°C and $-0.2 \text{ mm}/\text{day}$. It is warmer and wetter for CSTD, CCTU and CNLW by about $+1.5^{\circ}\text{C}$ and $+0.07 \text{ mm}/\text{day}$, $+0.6^{\circ}\text{C}$ and $+0.05 \text{ mm}/\text{day}$ and $+1.7^{\circ}\text{C}$ and $+0.12 \text{ mm}/\text{day}$ respectively.

4.2 Response of the coupled system to a global change in drag exchange coefficient

To analyze further the ocean–atmosphere feedbacks in terms of spatial patterns, we consider first the CSTD simulation. Compared to CREF, it represents the case where C_H is reduced by a factor 0.8 (Table 1). In addition, this simulation is at equilibrium with almost no drift in SST. As can be deduced from the AGCM simulation, the modification of the transfer coefficient in CSTD does not impact the wind. The

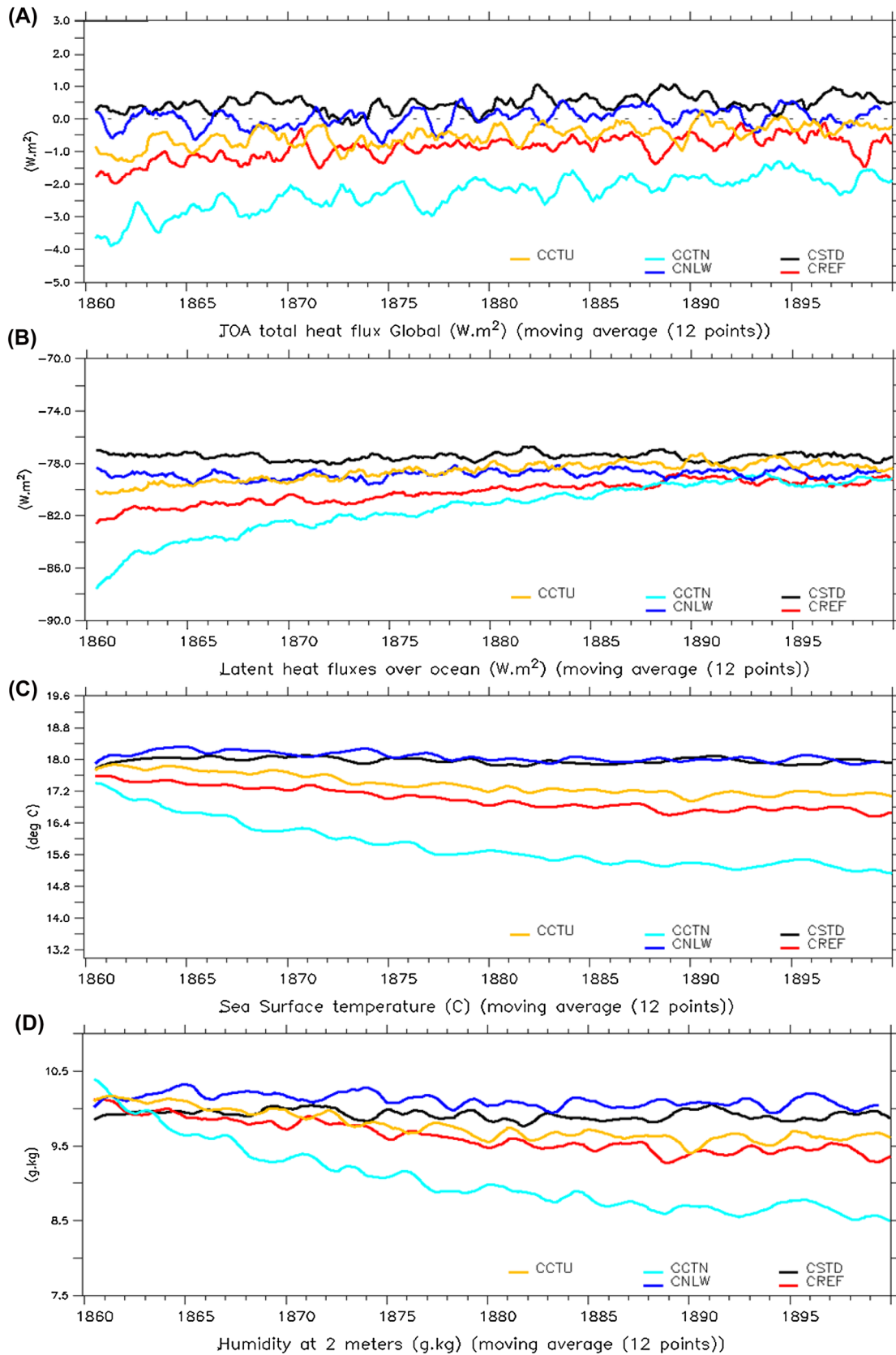


Fig. 11 Temporal evolution of the spatial averages (over the whole domain) for **a** atmospheric net radiative flux at the top of the atmosphere (W/m^2), **b** latent heat flux over ocean (W/m^2), **c** sea surface temperature ($^{\circ}C$) and **d** humidity at 2 m (g/kg) for OAGCM's simulations

Fig. 12 Annual mean differences on net surface flux and its different components in two boxes for CSTD and CNLW compared to CREF. The west box correspond to a spatial average between 30°N, 30°S and 80°–180°E while the east box correspond to a spatial average between 30°N–30°S and 180°–80°W

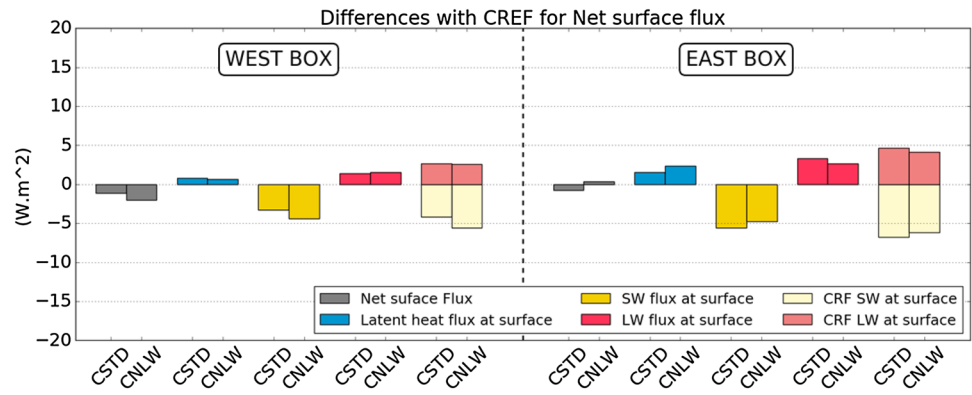
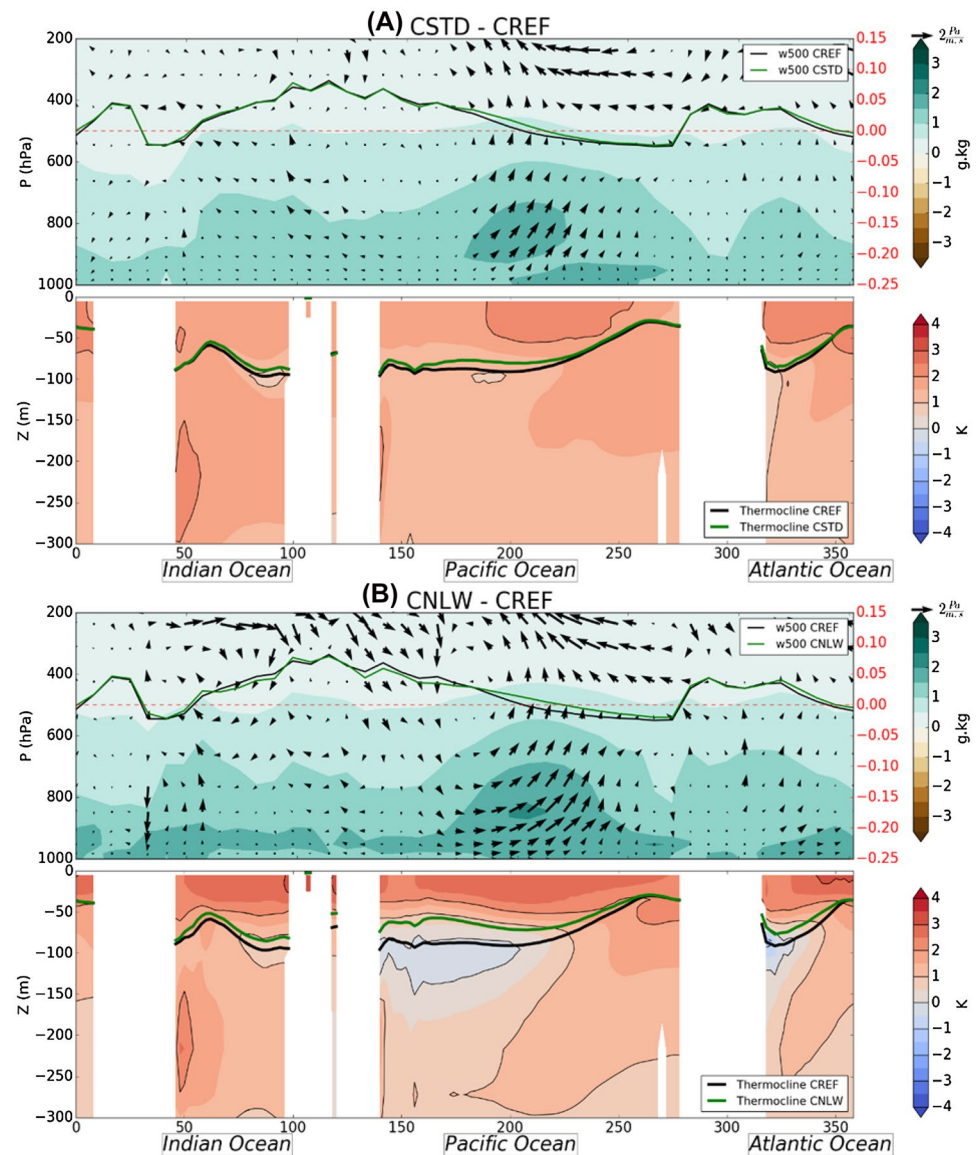


Fig. 13 Annual mean differences between **a** CSTD and CREF and **b** CNLW and CREF averaged between 5°N and 5°S. (Top) atmospheric vertical section for humidity (colors, g/kg), wind (arrows, Pa/m s) and vertical velocity at 500 hPa where the black lines stands for the reference simulation (CFAC) and the green line for the sensitivity experiment (Pa/s). Note that on these figure the vertical velocity has been magnified by a factor 100 and the sign has been reversed so that descending (ascending) arrows indicate subsidence (ascent). (Bottom) oceanic vertical section for differences in temperature (colors, °C) and thermocline depth (m) where the black lines stands for the reference simulation (CFAC) and the green line for the sensitivity experiment



modification observed is therefore due to a direct effect of the latent heat flux. Compared to CREF, the SST is warmer in order to release almost the same amount of latent heat flux at the global scale and achieve global radiative balance. Figure 13a presents a vertical section of the atmosphere–ocean circulation differences with CREF along the equatorial band (5°S–5°N). At the beginning of the simulation, decreasing the heat transfer coefficient diminishes the latent heat flux and reduced the evaporation everywhere. This reduces the energy transfer from the ocean to the atmosphere, leading to decreased evaporative cooling until a new, warm equilibrium is reached. Despite very small differences in net and latent heat fluxes between CSTD and CREF in the west and the east Pacific (-1.15 , 0.83 W m^{-2} in the west box and 0.73 , 1.51 W m^{-2} in the east box define in Sect. 3.1 for net and latent heat flux respectively, Fig. 12) the SST response is larger in the eastern part of the Pacific where the thermocline is shallower. It reaches $+1.4 \text{ K}$ in the west box (as given in Sect. 3.1) and $+1.81 \text{ K}$ in the east box, which reduces the temperature gradient along the equator. Trade winds are very similar in the west box and slightly decreased by 0.05 m s^{-1} in the east box, which in turn decreases evaporation and SST cooling. This mechanism is similar to positive wind–evaporation–SST (WES) feedbacks (Xie and Philander 1994) especially if we combine CH and wind into an evaporative efficiency where the effect of CH decrease is equivalent to the effect of reduced wind on evaporation (Eq. 1). It has been shown that the WES feedbacks are positive when surface temperature and zonal wind variations are in phase with westerly (easterly) wind anomalies overlying warm (cold) SST anomalies (Kossin and Vimont 2007; Xie 1999).

The establishment of the WES feedback causes the appearance of another important feedback, the Bjerknes feedback. Bjerknes (1969) gave the name “Walker Circulation” to the east–west convection cell and related it to SST (Kousky et al. 1984). As stated previously, in the CSTD simulation, trade winds are weakened in the eastern and central Pacific. The dynamical effect of wind reduces the tilt of the thermocline. Its depth shoals by 7 m in the central Pacific. This leads to reduced upwelling, a slowdown in ocean circulation and increased SSTs in the region. This reinforces locally the surface warming and causes an increase of lower-tropospheric moisture through latent heat and increased moisture convergence. This strengthens ascending motion through enhanced diabatic heating and the combination of these two feedbacks and of the modification of humidity gradient explains the slight extent to the east of the walker cell (over warm SST) in this case and the maximum humidity differences found in the central Pacific (Fig. 13a).

After adjustment occurs, the net surface and latent heat flux differences observed in AGCM between ASTD and AREF largely disappear (Fig. 12). The surface has a similar net heat budget between the two simulations. However,

radiative fluxes indicate that the atmospheric circulation is different (Fig. 12). As for AGCM simulations, the short-wave CRF has strong impacts (-4.18 in the west box and -6.76 W m^{-2} in the east box define in Sect. 3.1) but unlike AGCM simulations it is balanced by the long-wave CRF (2.64 in the west and 4.63 W m^{-2} in the east box). This highlights that changes in cloud cover have a larger role than water vapour and counteract the LW greenhouse effect. The net surface flux confirms that the changes observed in the OAGCM simulations are controlled by the modification of the circulation. It also show that the ocean absorbs almost all the perturbation produced by the modification of the transfer coefficient. However, as with the AGCM simulations, the west and east Pacific basins respond differently (Fig. 12).

The differences in the atmospheric column between AGCM and OAGCM simulations have their counterpart in the differences in MSE transport. Figure 14 shows that the MSE export is enhanced over the eastern part of the Pacific and an E/W structure, not observed in AGCM appears for CSTD compared to CREF (Fig. 14a). This is consistent with the warming of tropical SST's, which is stronger in the eastern part of the Pacific and increases the ocean heat available for the atmosphere. It is also consistent with the extent to the east of the ascending branch of the Walker's cell (Fig. 13a). This can be interpreted as more energy being transferred into the Indian and western Pacific from the eastern Pacific and the Atlantic. As shown in Fig. 14b, the impact of the Lq export is very low due to the adjustment which causes a similar latent heat flux between CSTD and CREF.

For CCTN, which also responds to a uniform change in C_H the same mechanisms operate but the opposite sign is observed. Increased C_H cools the upper ocean leading to a decrease of atmospheric humidity, an enhancement of the westward wind and a deepening of the thermocline of about 40 m in the center of the Pacific Ocean. In this simulation the same feedbacks are active but with an opposite sign and reinforced effects. This amplitude difference is seen in Fig. 16 which show a spatial distribution in boxplot form of the annual mean differences in MSE potential compared to their respective references (AREF and CREF) in the two different boxes define in Sect. 3.1. As with CSTD, in the CCTN simulation the east box is the most impacted but the sign is opposite and the amplitude is much higher.

4.3 Response of the coupled system to a regional change in drag exchange coefficient

To study the ocean–atmosphere system response to a regional change in heat drag coefficient (in the warm pool region), we consider the ANLW simulation. Compared to CREF, this simulation represents the case where the low wind speed parameterization used to compute C_H is removed. As for CSTD, the SST is higher compared to

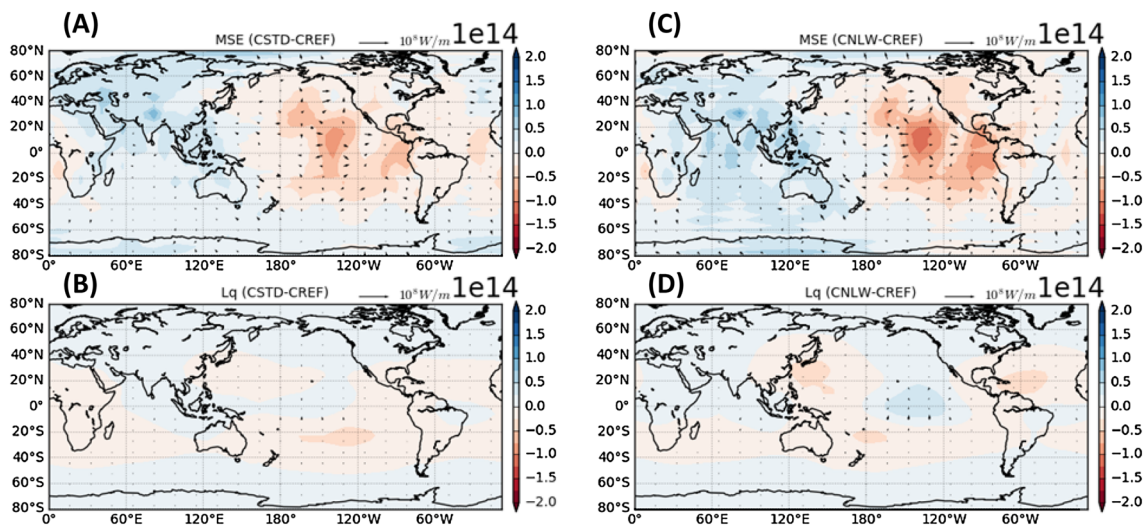


Fig. 14 Differences on the annual mean MSE and Lq transport by the atmosphere (arrows, W/m) and MSE and Lq potential (colors, W) between **a, b** CSTD and CREF and **c, d** CNLW and CREF. Arrows

CREF in order to release almost the same amount of latent heat at the global scale and achieve radiative balance. Figure 13b presents a vertical section of the atmosphere–ocean circulation differences with CREF along the equatorial band (5°N – 5°S). At the beginning of the simulation, decreasing the heat transfer coefficient diminishes the latent heat flux and reduces the evaporation predominately in the west of the Pacific basin where low winds are found. This effect is amplified by radiative feedbacks (Fig. 12) which further reduce the energy transfer from the ocean to the atmosphere. This warms and stratifies the ocean and shoals the thermocline depth by 18 m in the west Pacific, until a new warm equilibrium is reached. As observed in the AGCM simulation, trade winds are reduced (-0.13 m s in the east box defined in Sect. 3.1 and -0.06 m s in the west box), which in turn decreases the moisture advection from the east to the west of the Pacific and decreases evaporation and SST cooling. As for a global modification, this mechanism is similar to positive wind–evaporation–SST (WES) feedbacks (Xie and Philander 1994). The establishing of the feedbacks differs from CSTD simulation (Sect. 4.2) due to the direct impact of a regional modification on the wind which has a direct effect on temperature through Bjerknes (1969) feedback. Despite similar net heat flux and thermocline depth between the east and the west Pacific in the CNLW simulation, due to the wind response, the SST response is slightly larger in the eastern part of the Pacific ($+1.96$ K in the east box defined in Sect. 3.1) than in the western part ($+1.64$ K in the west box). In this case the Bjerknes feedback is active from the beginning of the simulation, explaining why the thermocline change is larger in CNLW than is CSTD. As with the CSTD simulation, the adjustment produces a

are draw every 2 points on X and Y axis and continents are masked because of the too noisy continental signal due to low resolution

moistening of the lower troposphere (with a maximum in the middle of the Pacific). However, the effect on the ocean on the other part is different, it is much more stratified and slightly warmer at the surface for CNLW (Fig. 13) which causes a shift in Walker circulation and not only an extent (Fig. 13b). This indicates the dampening effect of the ocean in the ocean–atmosphere adjustment.

Figure 14c presents long-term mean changes in MSE potential export for CNLW compared to CREF. The mean MSE export is enhanced over the eastern part of the Pacific. This is consistent with the warming of tropical SST's and also with the strengthening and shifted to the east Walker circulation. As for CSTD, the impact of the Lq potential export is limited (Fig. 14d). When the low wind speed parameterization is suppressed, the same behavior is observed between OAGCM and AGCM simulations for the MSE export differences (Figs. 8c, 14c), but with lower amplitudes due to the dampening effect of the ocean. The same E/W structure is observed due to the same response of wind. This implies that it is not because we have a change in latent heat flux sign that we observe an inversion in the heat transport pattern. In this case, when the modification is regional, the change in latent heat flux does not counteract the radiative fluxes. As with the AGCM simulation, more energy is transferred into the Indian and western Pacific from the eastern Pacific and the Atlantic. For CCTU (not shown), similar features emerge but with a lower intensity. These amplitude differences are shown Fig. 16.

As previously explained, the adjustment that occurs between the ocean and the atmosphere leads to a similar atmospheric state for CNLW and CSTD. This results in almost identical zonal heat transport by the atmosphere

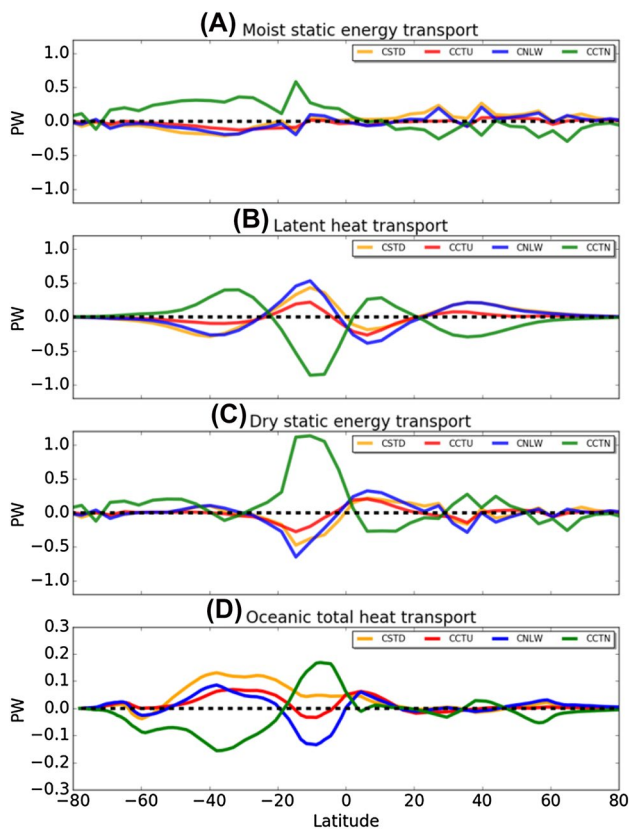


Fig. 15 Differences of the annual mean. **a** MSE transport by the atmosphere (PW), **b** atmospheric latent heat transport (PW), **c** dry static energy transport (PW) and **d** oceanic heat transport (PW) between CSTD, CCTN, CCTU, CNLW and CREF

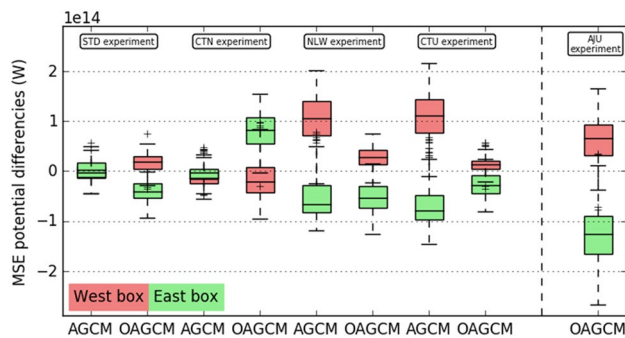


Fig. 16 Spatial distribution in form of boxplot of the annual mean differences of MSE potential export by the atmosphere (W) between 30°S and 30°N in two different boxes in the Pacific region (40°–180°E for the west boxes and 180°–80°W for the east boxes) for all the simulations (AGCM and OAGCM) compared to their respective references (AREF and CREF)

for these simulations compared to the reference (CREF), with only oceanic heat transport differing (Fig. 15). Unlike AGCM simulations, the latitude of the maximum difference in latent heat transport is similar for all sensitivity

experiments. The asymmetries observed in AGCM are not present in the OAGCM simulations, only the amplitude changes between the simulations compared to the reference (CREF) for atmospheric heat transport. However, as in AGCM simulations, the more the atmospheric circulation is impacted the greater the difference in the equator-to-pole export of energy. For the coupled model, the largest modification of equator-to-pole heat transport is obtained for the CCTN simulation (Fig. 15).

4.4 Impact of atmospheric model tuning

In a fully coupled model the response to a perturbation is difficult to predict, the adjustment that takes place between the ocean and atmosphere is, on the other hand, an understandable phenomenon. Găinușă-Bogdan et al. (2018) highlights the link between the pattern of the latent heat flux biases in stand-alone models and the systematically and negatively correlated pattern of SST biases in coupled simulations. The comparison between atmosphere stand-alone and coupled simulations indicates that this holds in our simulations. The patterns are different from those found in Găinușă-Bogdan et al. (2018) due to the fact that we compare simulations and in the initial study they compared simulations with observations. Here we find the strongest link between differences in SST in coupled simulation and differences in latent heat flux in atmosphere stand-alone simulation around the warm pool and in the Atlantic and Indian oceans. With an imposed SST field, errors or modification in the atmospheric stand-alone model impact directly on the distribution of other variables such as latent heat flux while in the coupled model, when the SST is allowed to develop, the same atmospheric modification or errors are transferred to the SST field and heat is stored in the ocean. Moreover, as Potter et al. (2017) shows, SST changes are propagated by ocean currents and can therefore have a more long-term effect than flux changes, which are instantaneous. This phenomenon further complicates the response of a coupled ocean atmosphere model.

However, we must not forget that in a coupled model, to properly represent the Earth’s energetics with the appropriate global temperature, tuning is always required (Hourdin et al. 2016). Some of the changes we highlight in the sensitivity experiments to the heat drag coefficient lead to unrealistic climate temperatures that are too warm or too cold compared to modern observations (Fig. 12). To explore if model tuning realized to adjust the overall energy balance modifies our main conclusions we performed a twin simulation to CCTN, named CAJU, in which some clouds parameters were adjusted to maintain a warmer temperature in the atmosphere. While CCTN has a global mean temperature of 9.73 °C, the adjustment brings it to a spatio-temporal average temperature at 2 m of 14.69 °C for CAJU. We recognize

this is a significant tuning, but it was performed within the range of atmospheric parameter uncertainties.

Figure 16 presents the results for the adjusted simulation (CAJU) compared to the reference used in this paper (CREF). Although the increase of transfer coefficient is similar between CCTN and CAJU the tuning leads to an opposite response of the system. The tuning of clouds to maintain the atmospheric temperature counteracts the cooling induced by the adjustment of the latent heat fluxes in CCTN. A strong increase of LH, humidity and therefore of the precipitation is observed (not shown). The comparison of CAJU and CREF shows that the western part of the Pacific Ocean transfer less energy (positive values). This is balanced by energy transfer from the Atlantic and the eastern part of the Pacific basin (negative values), and is the opposite of that found for CCTN. However, the east box remains the most impacted due to the global modification of the transfer coefficient in CAJU. By strengthening the ascending branch of the walker cells, the cloud tuning maintains more humidity in the upper layer of the atmosphere and increases the precipitations in all equatorial bands.

The adjustment counteracts the radiative imbalance in ACTN and maintains more energy in the system. In short, the tuning counterbalances the results obtained with the initial perturbation and modifies the feedbacks in the coupled model by bringing it closer to the atmosphere stand-alone model. When tuning is performed, in most cases, the impact of a parameterization modification is difficult to disentangle from other feedbacks that take place in a coupled system and there is a risk of assessing the effect of the tuning and not of the modification on the physical package.

5 Conclusion

The present study investigates the large scale impacts of the transfer coefficient used to compute turbulent heat fluxes, focusing on the tropical regions. This is a key area of the climate system that is important for the redistribution of energy between the equator and the poles (Kjellsson 2015; Saint-Lu et al. 2016). The latent heat flux provides energy to the evaporation process. It plays an important role in the water cycle (Cao et al. 2015) and the global ocean atmosphere circulation. To better understand how the representation of this flux affects the coupled ocean atmosphere system, we performed sensitivity experiments with a very low atmospheric resolution version of the IPSL-CM4 model in which the surface bulk formula is modified. Performing these tests with parallel atmospheric stand-alone and fully coupled ocean-atmosphere models allows us to study the direct effect of the disturbance with the AGCM and the mechanisms of adjustment to these changes between the ocean

and the atmosphere with the OAGCM. We focus on global energetics and the atmospheric circulation response.

An atmosphere stand-alone model reflects a direct response to the modification of the bulk formula. With an imposed SST, there is a clear link between latent heat flux, humidity and precipitation. A regional modification of heat transfer coefficient has more impact than a global modification due to the impact on large scale humidity and temperature gradients which give rise to pressure gradients that in turn cause modification of the wind and thereby the atmospheric circulation. A coupled model reacts differently to the same perturbation. Specifically, the modification of the transfer coefficient impacts the SST and atmospheric state variables but not directly the latent heat flux which must remain almost the same to achieve radiative balance. This modifies the way the coupled system works due to the link between atmospheric circulation and SST and the different feedbacks between ocean and atmosphere. Global impacts have more importance than regional impacts in this case. As shown in Fig. 16, the same areas are impacted in AGCM and OAGCM simulations. Regional changes have more impact in the west Pacific while global changes affect the east of the Pacific basin. This demonstrates that beyond the physical details of the model itself, the relationships between regions through large scale atmosphere ocean circulation are of critical importance in explaining the functioning of the global system.

The last key point highlighted in this study is that in climate models, although the importance of turbulent heat fluxes on the global system is recognized, it remains difficult to improve their representations to upgrade both the climatology of a coupled and a forced model. It is also difficult to understand the impacts of the parameterization of turbulent fluxes due to the sensitivity of atmospheric circulation to their representation, the different feedbacks between ocean and atmosphere and model tuning. For this reason, idealized studies are needed to understand how different parameterizations interact but also to avoid the risk of only assessing the effects of tuning when analyzing coupled simulations. It would be interesting to do further investigations on the role of latent heat flux on the clouds and how convection and cloud parameterization responds to surface change. This would help to further understand the differences between low and high atmospheric layers and thereby to better assess the role of this flux in balancing energetics in global climate models.

Acknowledgements This manuscript is a contribution to the ANR COCOA project (ANR-16-CE01-0007). Computing time was provided by GENCI (gen 2211) on the CURIE CCRT super computer using model. Computing and analysis tools are developed by the IPSL IGCM group. The simulations were performed as part of the DECLIC project (GIS climat DECLIC project). The lead author is supported by a CFR

PhD grant of the CEA (Commissariat à l'Énergie Atomique et aux énergies alternatives).

References

- Adler RF, Huffman GJ, Chang A, Ferraro R, Xie P, Janowiak J, Rudolf B, Schneider U, Curtis S, Bolvin D, Gruber A, Susskind J, Arkin P, Nelkin EJ (2003) The version 2 Global Precipitation Climatology Project (GPCP) Monthly Precipitation Analysis (1979–Present). *J Hydrometeorol* 4(6):1147–1167
- Barnier B (1998) Forcing the Ocean. In: Chassignet J, Verron EP (eds) *Ocean modeling and parameterization*. Kluwer Academic Publishers, The Netherlands. pp 45–80
- Beljaars ACM, Beljaars BACM. 1995. The parametrization of surface fluxes in large-scale models under free convection. *Q J R Meteorol Soc* 121(522):255–270. <https://doi.org/10.1002/qj.49712152203>
- Bellucci A, Gualdi S, Navarra A (2010) The double-ITCZ syndrome in coupled general circulation models: the role of large-scale vertical circulation regimes. *J Clim* 23(5):1127–1145
- Birol Kara A, Rochford PA, Hurlburt HE, 2000. Efficient and accurate bulk parameterizations of air–sea fluxes for use in general circulation models. *J Atmos Ocean Technol* 17(10), 1421–1438
- Bjerknes J (1969) Atmospheric teleconnections from the equatorial pacific. *Mon Weather Rev* 97(3):163–172. [https://doi.org/10.1175/1520-0493\(1969\)097<0163:ATFTEP>2.3.CO;2](https://doi.org/10.1175/1520-0493(1969)097<0163:ATFTEP>2.3.CO;2)
- Blanc TV (1985) Variation of bulk-derived surface flux, stability, and roughness results due to the use of different transfer coefficient schemes. *J Phys Oceanogr* 15(6):650–669. [https://doi.org/10.1175/1520-0485\(1985\)015<0650:VOBDSF>2.0.CO;2](https://doi.org/10.1175/1520-0485(1985)015<0650:VOBDSF>2.0.CO;2)
- Cao N, Ren B, Zheng J (2015) Evaluation of CMIP5 climate models in simulating 1979–2005 oceanic latent heat flux over the Pacific. *Adv Atmos Sci* 32(12):1603–1616
- Chahine MT (1992) The hydrological cycle and its influence on climate. *Nature* 359, 6394, 359(6394):373–380. <http://www.u.arizona.edu/~conniew1/geog532/Chahine1992.pdf%5Cnhttp://ntrs.nasa.gov/search.jsp?R=19930026415>
- Charnock H (1955) Wind stress on a water surface. *Q J Roy Meteorol Soc* 81:639–640. <https://doi.org/10.1029/2004JC002585>
- Chen D, Busalacchi AJ, Rothstein LM (1994) The roles of vertical mixing, solar radiation, and wind stress in a model simulation of the sea surface temperature seasonal cycle in the tropical Pacific Ocean. *J Geophys Res* 99(C10):20345. <http://rainbow.ldeo.columbia.edu/~dchen/collection-dchen/jgr94.pdf%5Cnpapers3://publication/uuid/162C05ED-3E74-401E-9D41-CA6EE1D24D43>
- Corrin S (1975) Limitations of gradient transport models in random walks and in turbulence. *Adv Geophys* 18(PA):25–60
- Covey C, Barron E (1988) The role of ocean heat transport in climatic change. *Earth-Sci Rev* 24(6):429–445
- DeCosmo J et al (1996) Air-sea exchange of water vapor and sensible heat: the humidity exchange over the sea (HEXOS) results. *J Geophys Res Oceans* 101(C5):12001–12016. <https://doi.org/10.1029/95JC03796>
- Fairall CW et al (2003) Bulk parameterization of air-sea fluxes: Updates and verification for the COARE algorithm. *J Clim* 16(4):571–591
- Fichefet T, Morales Maqueda MA (1999) Modelling the influence of snow accumulation and snow-ice formation on the seasonal cycle of the Antarctic sea-ice cover. *Clim Dyn* 15(4):251–268
- Găinușă-Bogdan A, Hourdin F, Khadre Traore A, Braconnot P (2018) Omens of coupled model biases in the CMIP5 AMIP simulations. *Clim Dyn*. <https://doi.org/10.1007/s00382-017-4057-3>
- Held IM, Soden BJ (2006) Robust responses of the hydrological cycle to global warming. *J Clim* 19(21):5686–5699
- Hourdin F et al (2006) The LMDZ4 general circulation model: climate performance and sensitivity to parametrized physics with emphasis on tropical convection. *Clim Dyn* 27(7–8):787–813
- Hourdin F et al (2015) Air moisture control on ocean surface temperature, hidden key to the warm bias enigma. *Geophys Res Lett* 42(24):10885–10893
- Hourdin F et al (2016) The art and science of climate model tuning. *Bull Am Meteorol Soc* 98. <https://doi.org/10.1175/BAMS-D-15-00135.1>
- Kjellsson J (2015) Weakening of the global atmospheric circulation with global warming. *Clim Dyn* 45(3–4):975–988
- Kossin JP, Vimont DJ (2007) A more general framework for understanding atlantic hurricane variability and trends. *Bull Am Meteorol Soc* 88(11):1767–1781
- Kousky VE, Kagano MT, Cavalcanti IFA (1984) A review of the Southern Oscillation: oceanic-atmospheric circulation changes and related rainfall anomalies. *Tellus A* 36A(5):490–504
- Krinner G (2005) A dynamic global vegetation model for studies of the coupled atmosphere-biosphere system. *Glob Biogeochem Cycles* 19:GB1015. <http://www.agu.org/pubs/crossref/2005/2003GB002199.shtml>
- Kubota M et al (2002) Japanese ocean flux data sets with use of remote sensing observations (J-OFURO). *J Oceanogr* 58(1):213–225
- Large WG, Pond S (1981) Open ocean momentum flux measurements in moderate to strong winds. *J Phys Oceanogr* 11(3):324–336
- Large WG, Yeager SG (2004) Diurnal to decadal global forcing for ocean and sea-ice models: the data sets and flux climatologies. NCAR Tech. Note, TN-460 + ST(May)
- Louis JF (1979) A parametric model of vertical eddy fluxes in the atmosphere. *Bound Layer Meteorol* 17(2):187–202
- Madec G et al (1998) OPA 8.1 ocean general circulation model reference manual. Notes du Pôle de Modélisation, Institut Pierre Simon Laplace no 11, p 97
- Marti O et al (2010) Key features of the IPSL ocean atmosphere model and its sensitivity to atmospheric resolution. *Clim Dyn* 34(1):1–26
- McGregor S et al. (2014) Recent Walker circulation strengthening and Pacific cooling amplified by Atlantic warming. *Nat Clim Change* 4(10):888–892. http://www.nature.com/nclimate/journal/v4/n10/full/nclimate2330.html?WT.ec_id=NCLIMATE-201410
- Miller MJ, Beljaars ACM, Palmer TN (1992) The sensitivity of the ECMWF? Model to the parameterization of evaporation from the tropical oceans. *J Clim* 5(5):418–434
- Minobe S, Kuwano-Yoshida A, Komori N, Xie S-P, Small RJ (2008) Influence of the Gulf Stream on the troposphere. *Nature* 452:206–209. <https://doi.org/10.1038/nature06690>
- Monin AS, Obukhov AM (1954) Basic laws of turbulent mixing in the atmosphere near the ground. *Tr Akad Nauk SSSR Geofiz Inst* 24:163–187
- Potter H, Drennan WM, Graber HC (2017) Upper ocean cooling and air-sea fluxes under typhoons: a case study. *J Geophys Res Oceans* 122(9):7237–7252
- Rayner NA (2003) Global analyses of sea surface temperature, sea ice, and night marine air temperature since the late nineteenth century. *J Geophys Res* 108(D14):4407. <https://doi.org/10.1029/2002JD002670>
- Redelsperger JL, Guichard F, Mondon S (2000) A parameterization of mesoscale enhancement of surface fluxes for large-scale models. *J Clim* 13(2):402–421
- Saint-Lu M, Braconnot P, Leloup J, Marti O (2016) The role of El Niño in the global energy redistribution: a case study in the mid-Holocene. *Clim Dyn*. <https://doi.org/10.1007/s00382-016-3266-5>
- Seager R, Blumenthal MB, Kushnir Y (1995) An advective atmospheric mixed layer model for ocean modeling purposes: global simulation of surface heat fluxes. *J Clim* 8(8):1951–1964

- Smith SD (1988) Coefficients for sea surface wind stress, heat flux, and wind profiles as a function of wind speed and temperature. *J Geophys Res* 93(C12):15467–15472
- Stull RB (1988). An introduction to boundary layer meteorology. Kluwer Academic Publishers, Dordrecht
- Swenson MS, Hansen DV (1999) Tropical Pacific Ocean mixed layer heat budget: the Pacific cold tongue. *J Phys Oceanogr* 29(1):69–81
- Trenberth KE (1995) Atmospheric circulation climate changes. *Clim Change* 31(2–4):427–453
- Trenberth KE, Stepaniak DP (2004) The flow of energy through the earth's climate system. *Q J R Meteorol Soc* 130(603 PART B):2677–2701
- Uppala SM et al (2005) The ERA-40 re-analysis. *Q J R Meteorol Soc* 131:2961–3012
- Xie SP (1999) A dynamic ocean-atmosphere model of the tropical Atlantic decadal variability. *J Clim* 12(1):64–70
- Xie S, Philander SGH (1994) A coupled ocean-atmosphere model of relevance to the ITCZ in the eastern Pacific. *Tellus A* 46(4):340–350
- Zeng X, Zhao M, Dickinson RE (1998) Intercomparison of bulk aerodynamic algorithms for the computation of sea surface fluxes using TOGA COARE and TAO data. *J Clim* 11(10):2628–2644